Solar twins in M 67

Luca Pasquini, Katia Biazzo, Piercarlo Bonifacio, Sofia Randich, L. R. Bedin

A&A 489, 677–684 (2008)
DOI: 10.1051/0004-6361:200809714

Astronomy & Astrophysics

Solar twins in M 67⋆,⋆⋆

L. Pasquini[1], K. Biazzo[1,2], P. Bonifacio[3,4,5], S. Randich[6], and L. R. Bedin[7]

[1] ESO - European Southern Observatory, Karl-Schwarzschild-Strasse 3, 85748 Garching bei München, Germany
e-mail: lpasquin@eso.org
[2] Istituto Nazionale di Astrofisica, Osservatorio Astrofisico di Catania, via S. Sofia 78, 95123 Catania, Italy
[3] CIFIST, Marie Curie Excellence Team
[4] GEPI, Observatoire de Paris, CNRS, Université Paris Diderot, Place Jules Janssen, 92190 Meudon, France
[5] Istituto Nazionale di Astrofisica, Osservatorio Astronomico di Trieste, via Tiepolo 11, 34143 Trieste, Italy
[6] Istituto Nazionale di Astrofisica, Osservatorio Astrofisico di Arcetri, Largo E. Fermi 5, 50125 Firenze, Italy
[7] Space Telescope Science Institute, 3700 San Martin Drive, Baltimore, MD 21218, USA

Received 4 March 2008 / Accepted 25 June 2008

ABSTRACT

Context. The discovery of true solar analogs is fundamental to a better understanding of the Sun and of the solar system. Despite a number of efforts, this search has brought only limited results for field stars. The open cluster M 67 offers a unique opportunity to search for solar analogs, because its chemical composition and age are very similar to those of the Sun.
Aims. We analyse FLAMES spectra of a large number of M 67 main sequence stars to identify solar analogs in this cluster.
Methods. We first determined cluster members that are not likely binaries, by combining proper motions and radial velocity measurements. We concentrate our analysis on determining stellar effective temperature, using analyses of line-depth ratios and Hα wing and making a direct comparison to the solar spectrum obtained with the same instrument. We also computed the lithium abundance for all the stars.
Results. Ten stars have the temperature derived both by line-depth ratios and by the Hα wings within 100 K from the Sun. From these stars we derive, assuming a cluster reddening $E(B-V) = 0.041$, the solar color $(B-V)_\odot = 0.649 \pm 0.016$ and a cluster distance modulus of 9.63. Five stars are most similar (within 60 K) to the Sun and candidates to be true solar twins. These stars also have a low Li content, comparable to the photospheric abundance of the Sun, likely indicating a similar mixing evolution.
Conclusions. We find several candidates for the best solar analogs ever. These stars are amenable to further spectroscopic investigations and planet searches. The solar colors are determined with fairly high accuracy with an independent method, as is the cluster distance modulus.

Key words. stars: fundamental parameters – Galaxy: open clusters and associations: individual: M 67 – stars: late-type

1. Introduction

The specificity of the Sun and of our solar system has been the subject of active investigation over the past 5 decades. How typical is the Sun of a star of its age, mass, and chemical composition? How typical is that solar-type stars host planetary systems? Are they at all similar to ours?

The quest to find stellar analogs to the Sun has been going on for a long time (for an extensive review see, e.g., Cayrel de Strobel 1996), and it stems from the poor knowledge we have of the Sun when seen as a star and from how typical the Sun is of a G2 type star, for its age, chemical composition, and population. It is, however, after the discovery of the first exoplanets (Mayor & Queloz 1995) that this quest became even more compelling, because finding stars similar to our own would allow us to answer fundamental questions related to the origin of the solar system, the frequency of planetary systems similar to ours, and eventually the formation of life in other exoplanetary systems (Cayrel de Strobel 1996). The need to identify in the night sky solar proxies to be used for spectroscopic comparison is also diffuse, in particular for the analysis of small solar system bodies (Böhnhardt, private communication).

Among the most recent results in this research, Meléndez et al. (2006) use high-resolution, high signal-to-noise ratio Keck spectra to show that HD 98618 is a very close solar twin, and King et al. (2005) propose HD 143436 after analyzing 4 stars pre-selected from literature. These stars seem to compare well with the best known solar twin, HR 6060, first analyzed by Porto de Mello & da Silva (1997), and subsequently confirmed by Soubiran & Triaud (2004), who made a comparative study of several hundreds of ELODIE spectra. Finally, Meléndez & Ramírez (2007) shows that HIP 56948 is the best solar twin known to date both in stellar parameters and in chemical composition, and it includes a low lithium abundance.

The open cluster M 67 is a perfect target when searching for solar analogs. Recent chemical analyses (Tautvaišiene et al. 2000; Randich et al. 2006; Pace et al. 2008) show that this cluster has a chemical composition (not only Fe, but also all the other elements) that is extremely similar to the solar one, as close as allowed by the high precision of the measurements. The analysis has resulted in [Fe/H] = -0.03 ± 0.03 for Tautvaišiene et al. (2000), [Fe/H] = 0.03 ± 0.01 for Randich et al. (2006), and [Fe/H] = 0.03 ± 0.03 for Pace et al. (2008).

There are other two additional characteristics that make M 67 strategic. The first one is that all the age determinations give an age for this cluster encompassing that of the Sun (3.5–4.8 Gyr; Yadav et al. 2008), while the age determination for field stars is always uncertain. The second characteristic is

⋆ Based on observations collected at the ESO VLT, Paranal Observatory, Chile, program 278.D-5027(A).
⋆⋆ Appendix A is only available in electronic form at http://www.aanda.org

that M 67 is among the very few clusters showing Li-depleted G stars (Pasquini et al. 1997). This is an important point because, as pointed out by Cayrel de Strobel (1996), even if many stars appear to have most characteristics similar to the Sun, their Li abundance is usually 10 times higher than in our star. Since Li indicates of the complex interaction taking place in the past between the stellar external layers and the hotter interior, the choice of stars that share the same Li abundance with the Sun is an additional property to pinpoint the true analogs.

In our opinion, the search of analogs to the Sun and to the solar system can be performed in open clusters (OCs), which show a homogeneous age and chemical composition, common birth, and early dynamical environment. As a consequence, they provide an excellent laboratory for investigating the physics of solar stars and of planetary system evolution, besides being excellent probes of the structure and evolution of the Galactic disk.

M 67 is a rich cluster, therefore it provides us with the opportunity to find many star candidates sharing characteristics, and not only one. This is fundamental to obtaining some meaningful statistics, and the cluster hosts many main sequence (MS) stars of mass around the solar mass, which form a continuous distribution (Fig. 1).

Finding several solar analogs in M 67 will also help in providing an independent estimate of the solar colors, a quantity that still suffers from some relevant uncertainty (see, e.g., Holmberg et al. 2006), as well as an independent estimate of the distance modulus of the cluster.

The present paper is the culmination of work that has involved the chemical determination of this cluster (Randich et al. 2006; Pace et al. 2008), photometry and astrometry (Yadav et al. 2008) to obtain membership, and FLAMES/GIRAFFE high-resolution spectroscopy to clean this sample from binaries, and to look for the best solar analogs using the line-depth ratio method (Gray & Johanson 1991; Biazzo et al. 2007) and the wings of the Hα line (Cayrel de Strobel & Bentolila 1989) to determine accurate temperatures with respect to the Sun. In addition, the Li line is used to separate Li-rich from Li-poor stars.

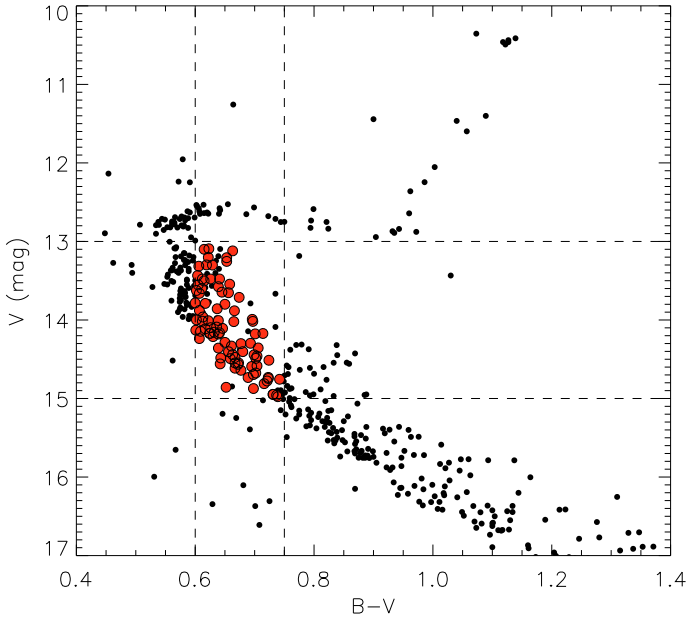

Fig. 1. Portion of the color-magnitude diagram of M 67. Our selected targets encompass the solar color, and are high probability proper motion (Yadav et al. 2008) and radial-velocity single members. The red points refer to the stars observed with FLAMES/GIRAFFE in three nights.

2. Observations and data reduction

We obtained 2.5 h in three observing nights in service mode with the DDT program 278.D-5027(A). Observations were carried out with the multi-object FLAMES/GIRAFFE spectrograph at the UT2/Kueyen ESO-VLT (Pasquini et al. 2002) in MEDUSA mode[1] and we were able to observe 90 targets (Table A.1). The setting was HR15N with central wavelength 665.0 nm, which with a wavelength range between 644 and 682 nm covers simultaneously the Hα and the Li I resonance doublet at 670.8 nm with a resolution of $R \sim 17\,000$. Three separate exposures were obtained to be able to identify short and intermediate period binaries by comparing the radial velocities at different epochs. The combined spectra have a typical signal-to-noise (S/N) ratio of 80–110/pixel.

From the catalog of Yadav et al. (2008) we selected the main sequence stars ($13\overset{m}{.}0 \lesssim V \lesssim 15\overset{m}{.}0$) with $B-V$ close to that of the Sun (≈0.60–0.75) with the best combination of proper motions parameters, that is a membership probability superior to 60%, and exclusion of candidates with a proper motion larger than 6 mas/yr with respect to the average cluster members. Full details about proper motion errors and selection criteria can be found in the original Yadav et al. (2008) work. The log of the observations is given in Table 1. The observations were reduced using the ESO-GIRAFFE pipeline.

Radial velocities were measured using the IRAF[2] package FXCOR, which cross-correlates the observed spectrum with a template. As a template we used a solar spectrum acquired with FLAMES/GIRAFFE. Finally, the heliocentric correction was applied. The typical error for our single measurement is around 0.4 km s^{-1}. The three spectra/star were finally co-added to perform the spectroscopic determination of temperature and lithium abundance (see Sects. 3.2 and 3.3).

We note that the GIRAFFE solar spectrum[3], taken with the same setup of our observations, is used through this work for spectroscopic comparison with the stars and the synthetic spectra. The solar spectrum has been obtained by averaging most of the GIRAFFE spectra (some show clear flat field problems and have not been used) and it has a nominal S/N above 400.

Table 1. Log of the observations.

α	δ	Date (d/m/y)	UT (h:m:s)	t_{exp} (s)	DIMM seeing (arcsec)
132.875	11.833	06/02/2007	06:24:29	2200	0.6
132.875	11.833	11/02/2007	04:01:08	2200	1.1
132.875	11.833	23/02/2007	01:34:55	2100	0.9

[1] This is the observing mode in FLAMES in which 132 fibers with a projected diameter on the sky of 1.″2 feed the GIRAFFE spectrograph. Some fibers are set on the target stars and others on the sky background.
[2] IRAF is distributed by the National Optical Astronomy Observatory, which is operated by the Association of the Universities for Research in Astronomy, Inc. (AURA) under cooperative agreement with the National Science Foundation.
[3] http://www.eso.org/observing/dfo/quality/GIRAFFE/pipeline/solar.html

Table 2. List of the six line pairs used to derive the stellar temperature.

λ_1/λ_2 (Å)	LDR	χ_1/χ_2 (eV)
6469.210/6456.380	FeI/FeII	4.84/3.90
6498.937/6516.050	FeI/FeII	0.96/2.89
6608.024/6597.557	FeI/FeI	2.28/4.80
6608.024/6627.540	FeI/FeI	2.28/4.55
6646.932/6627.540	FeI/FeI	2.61/4.55
6646.932/6653.850	FeI/FeI	2.61/4.15

3. Data analysis and membership

3.1. Radial velocity

Out of the 90 stars observed, all selected on the proper motion and membership criteria given above, we found that 59 of them are probable single radial-velocity (RV) members. We have retained all the stars that show RV variations smaller than ≈1 km s^{-1} in the three exposures acquired and that have a mean velocity within 2 sigma (≈1.8 km s^{-1}) from the median cluster RV. In Fig. 2 the histogram of the radial velocity distribution of these stars is shown, together with a Gaussian fit with $\langle V_{\rm rad}\rangle$ = 32.90 km s^{-1} and a σ = 0.73 km s^{-1}. In Table A.2 the RV values are listed for the stars of the final sample, while in the values of the single RV measurements are given Table A.3 for the stars we discarded.

In Fig. 3 we show the enlarged portion of the color-magnitude diagram (CMD) containing the original sample. In this figure the discarded and the retained stars are indicated with different colors. Many of the discarded stars tend to occupy the brighter side of the main sequence, where binaries are indeed expected to be present. On the other hand, our procedure still leaves several stars that are apparently above the photometric main sequence, because the radial velocity measurements are not of superb quality and because the time span by the observations is only 18 days. Long period binaries will not be discovered by our three radial velocity observations. We see that seven stars clearly stand up also in the Magnitude – Temperature diagram (see Fig. 5), and they are best candidates for binaries of similar mass. We kept them in the sample, and we anticipate that their presence does not influence our analysis or conclusions.

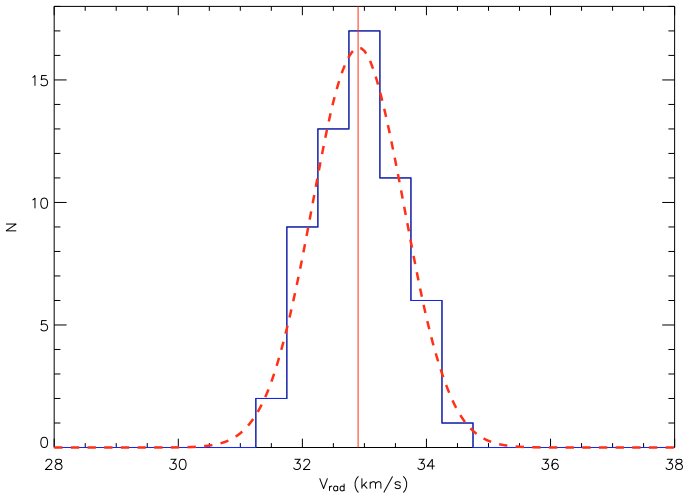

Fig. 2. Histogram of the radial velocity distribution of the 59 single members selected in M 67 (continuous line). A Gaussian fit to the member stars distribution is also displayed (dashed line).

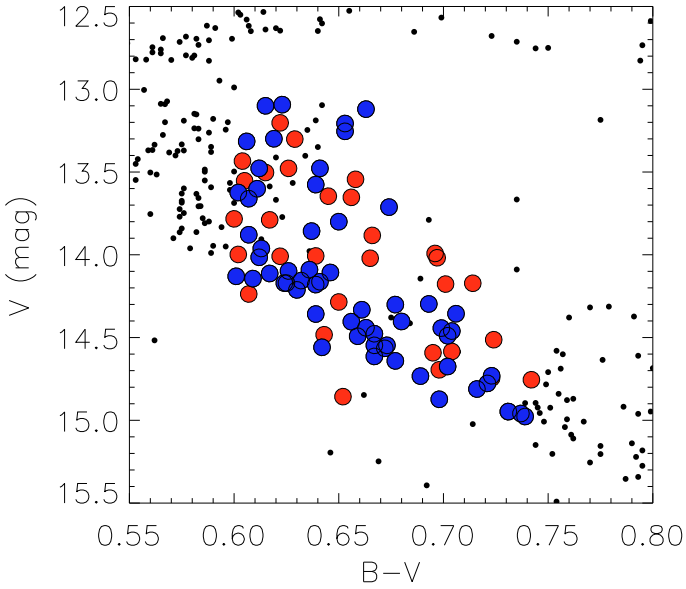

Fig. 3. Zoom of the M 67 CMD, centered on the targets observed. The 59 retained single member candidates are shown in blue, in red the discarded stars. As expected by binary contamination, most of the discarded stars lie on the bright side of the MS.

3.2. Effective temperature

Given that our targets are on the main sequence of a cluster with solar metallicity and age, the critical astrophysical parameter for the selection of the best solar analogs is the effective temperature. We used two spectroscopic methods to compute the stellar effective temperature: the line-depth ratios and the Hα wings. To calibrate these methods we used a grid of synthetic spectra, computed with SYNTHE from a grid of 1D LTE model atmospheres computed with version 9 of the ATLAS code (Kurucz 1993a,b) in its Linux version (Sbordone et al. 2004; Sbordone 2005). All the models were computed with the "NEW" Opacity Distribution Functions (Castelli & Kurucz 2003) that are based on solar abundances from Grevesse & Sauval (1998) with 1 km s^{-1} micro-turbulence, a mixing-length parameter $\alpha_{\rm MLT}$ of 1.25 and no overshooting. The grid of synthetic spectra covers the temperature range 5450–6300 K with [Fe/H] = 0, $\log g$ = 4.4377, ξ = 1 km s^{-1}, and was degraded to the resolution of the FLAMES/GIRAFFE spectra. We stress that for both methods these models are used to quantify the difference between the stellar spectra and the solar spectrum. Zero-point shifts are most likely present, due, for instance, to limitations in the atmospheric models or to imperfect treatment of the Hα lines. While these inaccuracies will be reflected in a wrong temperature for the Sun, the difference between the stars and the Sun will be much less affected.

3.2.1. LDR method

It has been demonstrated that, for stars with $B-V$ = 0.4–1.5, line-depth ratios (LDRs) are a powerful temperature indicator, capable to resolve temperature differences lower than 10 K (Gray & Johanson 1991; Catalano et al. 2002; Biazzo et al. 2007). Since our stars are within this $B-V$ range, we applied the LDR method to the members previously selected by radial velocity measurements (see Table A.2). To convert the line-depth ratios of our stars into effective temperature, we need to calibrate a temperature scale for the measured LDRs. To this purpose we

considered an initial sample of about 100 lines of iron group elements (which are usually temperature sensitive) present in the spectral range covered by our observations, from which we selected lines with the following characteristics: weak (to avoid saturation effects), sensitive to temperature variations, and measurable in our spectra. The final selection contains six line pairs suitable for applying the LDR method; we measured them in the synthetic spectra and then derived an LDR$-T_{\rm eff}$ calibration for each pair. In Table 2 we list for these six line pairs the wavelength, the element, and the excitation potential, as taken from the NIST[4] Atomic Spectra Database Lines, while in Fig. 4 we show an example of one LDR$-T_{\rm eff}$ calibration. The methods for the measurement of the line depth and the related uncertainties are described in Catalano et al. (2002) and Biazzo et al. (2007). In a summary, the lowest seven points in the core of each measured line were fitted with a cubic spline and the minimum of this cubic polynomial was taken as the line depth. Given the limited S/N and resolution, the errors in each line depth are dominated by the uncertainty of the signal in the continuum. We then measured the LDRs and derived the temperature for each line pair. In Table A.2 the averaged values for all line pairs are given, where the associated uncertainty reflects the scatter obtained by the six measurements.

With this method the effective temperature of the observed GIRAFFE solar spectrum results in 5792 ± 27 K, i.e. 15 K higher than the synthetic one (5777 K is the theoretical effective temperature of the solar atmosphere; Wilson & Hudson 1991).

We computed the temperature difference $\Delta T^{\rm LDR}$ between the FLAMES/GIRAFFE targets and the Sun (as obtained from the six line-depth ratios and the summed spectra of the targets) as a function of the de-reddened $B-V$ color ($E(B-V) = 0.041$; Taylor 2007). The $\Delta T^{\rm LDR}-(B-V)_0$ relationship for our targets is described well by a linear fit, which gives $\Delta T^{\rm LDR} = (-3662.65 \pm 351.22) \times (B-V)_0 + (2410.59 \pm 216.52)$ and an rms of 100 K.

In Fig. 5 the temperature-magnitude diagram is shown. The two colors of the symbols refer to stars with a lower and a higher presence of lithium. Seven stars clearly stand out of the main sequence, suggesting a parallel binary sequence. They most likely are long period binaries with components of similar mass not detected as RV variables by our observations, because of the limited time base of our observations.

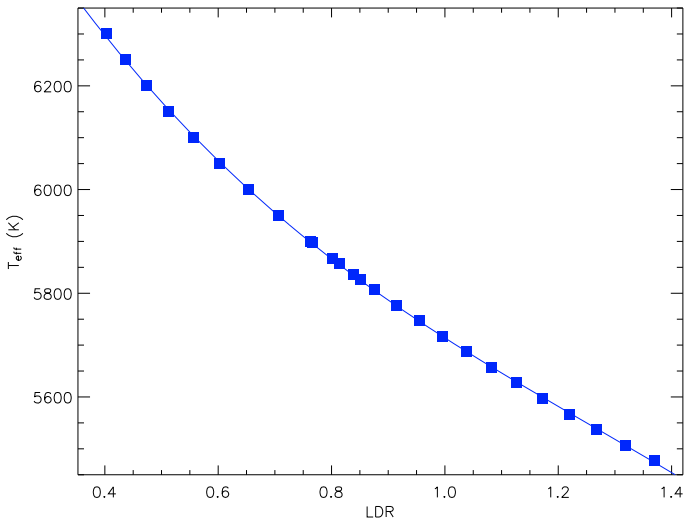

Fig. 4. Example of LDR$-T_{\rm eff}$ calibration obtained with synthetic spectra. The line-depth ratio is between λ6498.937 Å and λ6516.05 Å.

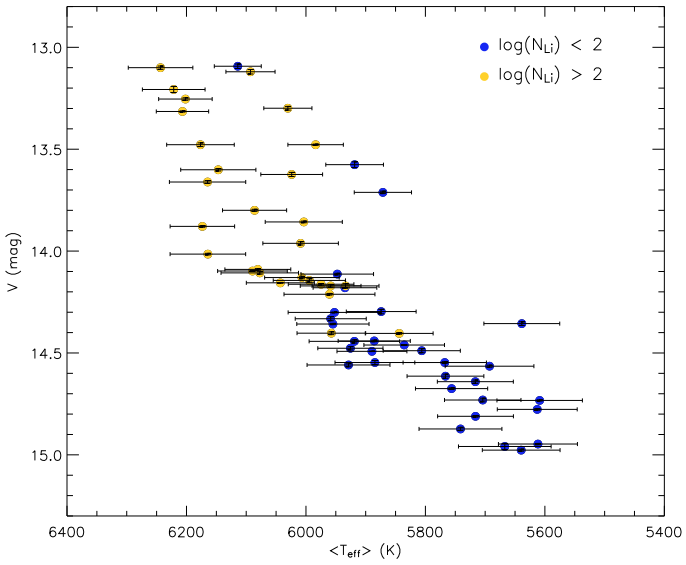

Fig. 5. V vs. $T_{\rm eff}$ of the probable candidates. The stars have different colors according to the LTE lithium abundance. Seven stars depart from the main sequence; they are most likely long period binaries that escaped the detection in our observations.

3.2.2. Hα line

The wings of the Hα line profile are very sensitive to temperature, like all the Balmer lines, and depend only slightly on metallicity and gravity (Cayrel et al. 1985; Fuhrmann et al. 1993; Barklem et al. 2002). In particular, the spectral region in the range between 3 and 5 Å of the Hα line center is a good effective temperature diagnostic (Cayrel de Strobel & Bentolila 1989). With respect to the higher members of the series, the Hα line has considerably less blending in the wings, making the placement of the continuum easier. A further advantage over other members of the series is its insensitivity to convection and in particular to the adopted mixing length parameter $\alpha_{\rm MLT}$ in 1D model atmospheres (Fuhrmann et al. 1993). Thus, we selected this region as a temperature indicator and for each star we compared the Hα line profile outside the core in our real spectrum against the synthetic profile. The hydrogen line profiles were computed in SYNTHE by routine `HPROF4`, which uses essentially the Ali & Griem (1965, 1966) theory for resonance broadening, and for Stark broadening it calls routine `SOFBET`, written by Deane Peterson, which uses essentially the theory of Griem (1960), with modified parameters, so as to provide a good approximation to the Vidal et al. (1973) profiles (F. Castelli, private communication). For more details on the computations of hydrogen lines in SYNTHE, see Castelli & Kurucz (2001) and Cowley & Castelli (2002). The dominant broadening for Hα is resonance broadening, while Stark broadening becomes relevant for higher members of the series. To minimize the subjectiveness of the measurement, we quantified the comparison between the synthetic profile and the observed one, minimizing the rms of the subtraction. Continuum normalization is not easy for such a broad line; however using a fiber instrument with a broad coverage minimize the subjectiveness of the process and makes it quite reproducible. Given the limited S/N of the observations, it is however very difficult to provide a realistic estimate of the involved uncertainties. The systematic errors in the

[4] National Institute of Standards and Technology.

effective temperature obtained from the Hα wings is given by Gratton et al. (2001), and the errors associated to the method have been discussed by, e.g., Bonifacio et al. (2007), where the dominant source of error for échelle spectra has been identified in residuals in the correction of the blaze function. The GIRAFFE spectra are fiber-fed, and the flat-field is obtained through the same optical path as the stellar spectra, thus flat-fielding allows better removal of the blaze function than is possible for slit spectra. We estimated an average error of ±100 K for our stars. With this method the effective temperature of the Sun results in 5717 ± 100 K, i.e. 60 K lower than the solar real value. We note that the absolute temperature determined in this way depends critically on a number of assumptions in the model and on the adopted broadening theory for Hα, and these produce a zero-point shift of the Sun. The relative measurements, which are made with respect to the observed solar spectrum, are instead rather insensitive to all the assumptions used to build the synthetic profile.

A linear fit describes the relationship between the temperature difference $\Delta T^{H\alpha}$ of the FLAMES/GIRAFFE targets and the Sun as obtained from the Hα wings, and the de-reddened $B-V$ color: $\Delta T^{H\alpha} = (-3811.8 \pm 283.39) \times (B-V)_0 + (2488 \pm 174.71)$ with an rms of 81 K.

The calibrations $\Delta T_{\rm eff}$ vs. $(B-V)_0$ obtained with the two methods agree quite closely, as shown in Fig. 7; they have slightly different slopes that produce a maximum difference at the red edge ($(B-V)_0 = 0.7$) of the sample of 40 K (Hα temperatures are cooler). These relationships can be used to calibrate stars with metallicity close to solar. Our LDR $T_{\rm eff}$ vs. $(B-V)_0$ relationship has almost exactly the same slope of the Alonso et al. (1996) relationship, but it is hotter than this by ~60 degrees. As a reference, the Alonso et al. (1996) scale produces an effective temperature for the Sun of 5730 K for a $B-V = 0.63$.

3.3. Lithium

Lithium is an important element because it is easily destroyed in stellar interiors, and its abundance indicates the amount of internal mixing in the stars. Lithium in Pop I old solar stars varies by a factor 10 (Pasquini et al. 1994), and M 67 is one of the few clusters that clearly shows this spread among otherwise similar stars (Pasquini et al. 1997).

Equivalent widths (EWs) of the lithium line at λ = 670.7876 nm were computed using the IRAF task SPLOT; from measured EWs, we derived Li abundances using the curves of growth (COGs) of Soderblom et al. (1993). At the GIRAFFE resolution, the Li I lines are blended with the Fe I λ670.744 nm line, whose contribution to the lithium blend was subtracted using the empirical correction of the same authors. Lithium abundances were then corrected for the NLTE effects using the prescriptions of Carlsson et al. (1994).

Figure 6 shows the lithium abundance (LTE and non-LTE) for the summed spectra of the 59 targets as a function of the effective temperature, as derived by the LDR method. The difference between LTE and non-LTE values is minor. The blue points are the solar twins (see Sect. 4). The position of the Sun is shown at $\log N({\rm Li})^{\rm LTE} = 0.84$ and $T_{\rm eff}^{\rm LDR} = 5792 \pm 27$ K (see Sect. 3.2). The lithium abundance is listed in Table A.2. Several solar twin candidates have Li abundances that are comparable to the Sun, whose value is 0.84 as measured by us on the GIRAFFE spectrum (see above), and 1.0 as measured in high-resolution solar atlas (Müller et al. 1975). In most investigations the error associated to the effective temperature is usually the dominant one (100 K correspond to about 0.1 dex in $\log N({\rm Li})$), but in this

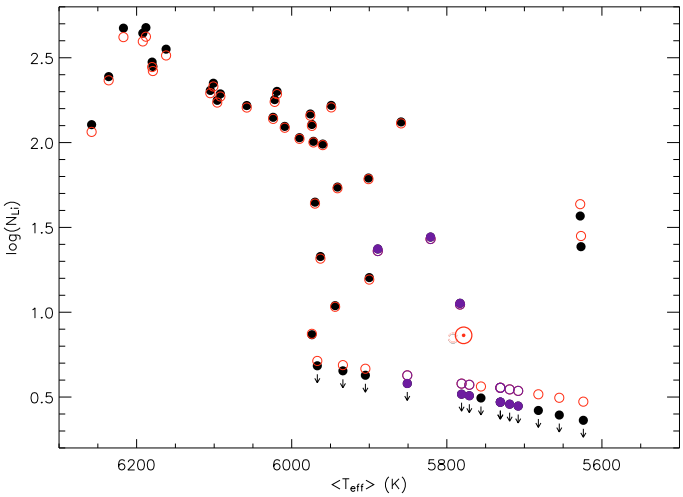

Fig. 6. Lithium abundance versus $T_{\rm eff}^{\rm LDR}$ for the most probable single stars observed in M 67. Filled circles: LTE abundances. Open circles: NLTE abundances. The blue points indicate the best solar analogs candidates. The position of the Sun is also shown at $\log N({\rm Li})^{\rm LTE} = 0.842$ and $T_{\rm eff}^{\rm LDR} = 5792 \pm 27$ K.

case, since we have good $T_{\rm eff}$ determination, but limited resolution and S/N, the uncertainty in the abundance associated to the equivalent width measurements is not negligible. The expected uncertainty in the measured lithium equivalent widths has been estimated from Cayrel (1988)'s formula:

$$\sigma_{\rm EW_{Li}} = \frac{1.6}{S/N} \sqrt{FWHM \times \delta x}$$

where S/N is per pixel, $FWHM$ is the full width of the line at half maximum, and δx the pixel size. The predicted accuracy, $\sigma_{\rm EW_{Li}}$, is 3.0 mÅ for a typical S/N of 80 and of 1.6 mÅ for a S/N of 150. However, it should be noted that this formula neglects the uncertainty on the continuum placement. We estimate that, using homogeneous procedures to determine the continuum and the line widths, the statistical error for the weak lithium line is on the order of 2–3 mÅ, depending on the S/N of the co-added spectrum. This will correspond to an asymmetric error $\Delta \log N({\rm Li}) \sim^{+0.3}_{-0.8}$ dex for a star with a line as weak as the Sun and ±0.04 dex for a star with a $\log N({\rm Li}) = 2.2$. Since the line is weak, the error (in percentage) is inversely proportional to the line strength. Given the errors, all the stars with upper limits in our sample may have a Li comparable to the solar one.

After the early works on M 67, several Li surveys have been carried out of additional clusters sampling the age metallicity space well (Randich 2008, and references therein). Out of nine clusters older than the Hyades with available Li measurements, only two, besides M 67, show a significant dispersion. The latter seems to be an exception, rather than a rule, and its occurrence depends neither on age nor on metallicity nor on global cluster parameters. In this context, the novel result of our analysis and, in particular, of the careful selection and cleaning of the sample, as well as of the precise effective temperature determination, is that the wide spread is clearly present only for stars cooler than ~6000 K. Stars warmer than 6200 K seem to show a decay, probably indicating the red side of the "Li-gap", while stars in the $6000 \leq T_{\rm eff} \leq 6200$ K do not show any major scatter.

It has now been ascertained on empirical grounds that, in order to explain the MS Li depletion in solar-type stars, an extra or non-standard mixing mechanism must be at work. No consensus has so far been found on the nature of this mechanism; it is

nevertheless clear that, whatever this process is, it must be driven by an additional stellar parameter besides mass and chemical composition. The presence of the Li spread indeed indicates that this parameter must vary from star to star and that, depending on it, some stars (including the Sun) undergo a much more efficient mixing than others, while the absence of a dispersion for stars warmer than 6000 K suggests that this parameter is more uniform among F-type stars.

Recent modeling have had some success in reproducing the solar Li abundance by using fairly complex models which include internal gravity waves (Charbonnel & Talon 2005), however, those models are not able to reproduce the observed evolution of Li with age and, in particular, the "plateau" in Li abundances at old ages (Randich 2008). We are not aware of similar models for a grid of masses to be compared to our observations; since the number of possible parameters which influence the Li evolution is very large (depth of convective zone, initial rotation, magnetic field, mass losses, and torques, just to mention a few), we cannot really predict at present why the extra mixing takes places at a given $T_{\rm eff}$ in M 67 stars.

4. Solar analogs

With the aim of finding the best solar analogs, we compared $\Delta T^{\rm LDR}$ to $\Delta T^{\rm H\alpha}$ (Fig. 7).

There are 10 stars in our sample for which both the $T^{\rm LDR}_{\rm eff}$ and $T^{\rm H\alpha}_{\rm eff}$ are within 100 K of the solar values (285, 637, 1101, 1194, 1303, 1304, 1315, 1392, 1787, 2018). We use these stars to find the best solar analogs and our best evaluation for the solar colors and the cluster distance. These stars are indicated in bold face in Table A.2.

The average difference between these 10 stars and the solar $T^{\rm LDR}_{\rm eff}$ is of −13 K (with a sigma of 60 K), while the average $T^{\rm H\alpha}_{\rm eff} - T^{\rm H\alpha,\odot}_{\rm eff}$ is =−9 K, with a sigma of 58 K. The average characteristics of these 10 stars should therefore represent the solar values.

The average $B - V$ of the ten analogs is $\langle B - V\rangle = 0.692$ ($\sigma = 0.020$), their average magnitude is $\langle V\rangle = 14.583$ mag ($\sigma = 0.147$), and the $\langle V - I\rangle = 0.754$ ($\sigma = 0.025$). The $B - V$ spread is broader than the formal errors in the photometry, indicating a possible real spread in the stellar characteristics. This is not surprising because, formally, these stars may span a range of up to 200 K in temperature.

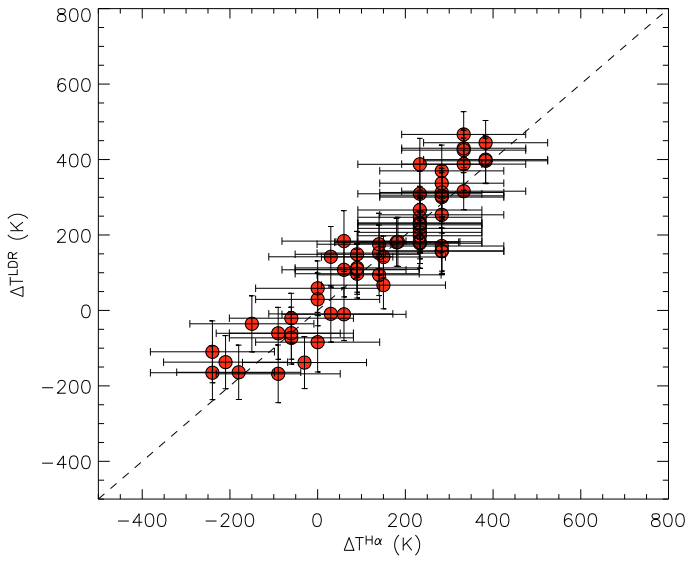

Fig. 7. $\Delta T^{\rm LDR}$ as a function of $\Delta T^{\rm H\alpha}$ for the 59 probable single member stars.

If we take our results in Table A.1, two stars (637 and 1787) have both $T_{\rm eff}$ determinations within 50 K from the solar values, and three additional ones (285, 1101, 1194) within 60 K; these 5 stars are overall the closest to the Sun, with nominal effective temperatures derived with both methods differing less than 60 K from the solar one. Their average magnitude (14.557 mag) is very similar to what is found for the full subsample of 10, as well as their average $B - V$ color (0.688) just 0.007 mag bluer than the whole subsample.

All the data in our possession indicate that some of these stars have a metallicity very close (within 0.03 dex; note that also their Li abundance is comparable; see previous section) to the Sun, that they have a very similar temperature (within 50 K), as well as a comparable age to the Sun, and that they are true main sequence stars. To the best of our knowledge they are the best candidates in M 67 to be the closest analogs to our star.

In Fig. 8 we compare the GIRAFFE spectrum of the Sun with the sum of the spectra of the 10 best star analogs and of the 5 best analogs in a portion of the spectra that includes Hα and in another including the Li lines. The extremely small difference between the solar spectrum and these co-added spectra quantitatively confirm the very close resemblance of these stars to the Sun.

At the request of the referee we also performed a direct comparison between the solar spectrum and the spectrum of our solar analogs. We used a χ^2 minimization with a Doppler shift and a re-adjustment of the continuum of the stars of M 67 as free parameters, in order to match the observed spectra to the observed GIRAFFE solar spectrum. The reduced χ^2 of the fit, or the associated probability, then provides a means to rank the M 67 stars. We restricted the comparison to a range of 10 Å centered on Hα. While in the fitting of the synthetic spectra the core of the line was excluded from the fitting range, it was included here. The LTE synthetic spectra fail to reproduce the core of Hα due to the presence of a chromosphere (absent in the model atmospheres employed by us) and to NLTE effects. Instead, the sought-for solar analogs must behave exactly like the Sun, including in the core of Hα. With this method the three M 67 stars that are most similar to the Sun are the stars 1194, 1101, and 637. The result is thus very similar to what is obtained by comparing the observed spectra to synthetic spectra, confirming that the stars we selected are very similar to the Sun. We prefer the method based on synthetic spectra, since the direct comparison to the solar spectrum is affected by the noise present in the latter.

5. Solar color

We would finally like to use the observed $B-V$ color of the solar analogs to derive the $B - V$ color of the Sun in an independent way, and this requires evaluating the cluster reddening.

The reddening towards M 67 has been evaluated by many authors in the past 50 years, and a thorough discussion is given by Taylor (2007). M 67 reddening is evaluated by this author in $E(B - V) = 0.041 \pm 0.004$, which is accidentally the same value as obtained by An et al. (2007) as the average point of the traditionally accepted range for the cluster. We therefore adopt this value. This implies that the de-reddened color for the average of our 10 solar analogs is $(B-V)_\odot = 0.651$. The value is in excellent agreement with what is found by inverting the fit of all the stars using the $T^{\rm LDR}$, which would have predicted $(B - V)_\odot = 0.659$, and the value obtained by inverting the fit of $T^{\rm H\alpha}$, which would give $(B - V)_\odot = 0.651$.

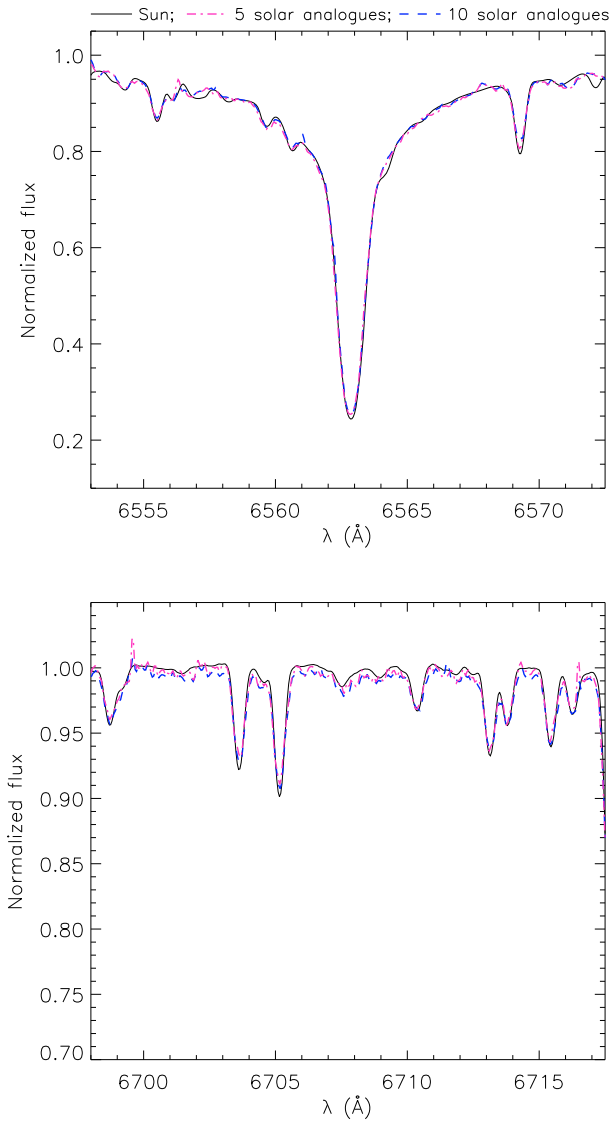

Fig. 8. Comparison between the GIRAFFE solar spectrum and the spectra of the 10 and 5 best solar analogs. The Hα and lithium regions are shown in the upper and bottom panels, respectively.

It is not simple to evaluate a realistic error estimate for this color. This should include: the spread (0.020 mag) around our determination, the uncertainty in the cluster reddening, plus other systematics originating from stellar evolution and photometry. We evaluated the evolutionary effects by investigating the expected variations of the solar color with age and metallicity by using evolutionary models. Photometric uncertainties are estimated by comparing Yadav et al. (2008) photometry with what has been obtained for this cluster by other groups.

We use the tracks from Girardi et al. (2000) for analyzing differential evolutionary effects. Because our stars have a similar effective temperature to the Sun, age has no influence; for stars younger than 5 Gyr of solar $T_{\rm eff}$, the visual absolute magnitudes and colors do not change in any appreciable way. If M 67 were younger than the Sun, the only effect would be that the masses of our stars were higher than the solar one by about 1%, but no difference is predicted in magnitude or colors. The other source of systematic uncertainty is the possibility that metallicity is not exactly solar. In this case, for a fixed effective temperature, we do expect that a star that is more metal rich by 0.05 dex would be slightly brighter (0.08 mag in V) and slightly redder (0.01 mag) than the Sun.

Our photometry comes from by Yadav et al. (2008), which was calibrated on stars observed in Sandquist et al. (2004). To check for photometric systematic errors, we compared our values for the 10 best analogs with Montgomery et al. (1993), finding that if using their photometry an average $(B-V)_0 = 0.650$ would have been found, i.e. only 1 mmag bluer than our value. Sandquist et al. (2004) made, on the other hand, a general comparison between his colors and those of Montgomery et al. (1993), finding an overall zero-point shift in $B-V$ of 8 mmag (the Sandquist' $B-V$ are bluer than the Montgomery ones). That the agreement for these 10 solar stars is better than this systematic shift might be due to a statistical fluctuation. It is on the other hand quite common that calibrations agree best for solar stars. We will nevertheless consider a 0.008 uncertainty in the color as introduced by the adopted photometry.

The simple average of the most recent estimate of the M 67 metallicity gives [Fe/H] = 0.01. This would require a correction of 2 mmag towards the blue for the solar colors derived from the M 67 stars to compensate for their higher metallicity. We conclude that a solar $(B-V)_\odot = 0.649 \pm 0.016$ is our present best estimate. The associated uncertainties are 0.006 mag given by the spread of our solar analogs divided by the square root of number of our solar analogs (namely 10); a 0.007 mag given by a generous uncertainty in the cluster metallicity (±0.03). Zero-points uncertainties in photometry are the dominant source and they account for 0.008. All these errors are summed quadratically. To this, the uncertainty in the cluster reddening determination, which is assumed to be 0.004 mag (Taylor 2007; An et al. 2007), is linearly added.

An additional hidden source of systematic effects, which might add a bias towards redder colors, might be present, and this is the presence of unidentified binaries. A typical red, faint companion will make the stars appear slightly brighter and slightly redder than what they should be, still influencing the spectroscopic $T_{\rm eff}$ determination very little. Given our radial velocity selection, only a few binaries should be left in our sample, and have low-mass companions. We cannot quantitatively account for their presence, but we keep this possibility in mind.

The $B-V$ value found is somewhat in the middle between the majority of the "old" determinations (see Table 2 of Barry et al. 1978, which found $\langle (B-V)_\odot \rangle = 0.667$ averaging most of the previous measurements) and the most recent determinations, which, as summarized, for instance, by Holmberg et al. (2006), tend to find $(B-V)_\odot$ in the range between 0.62 and 0.64. None of these results formally in disagree with ours, but we can exclude the estimates at the edges of the distribution.

We think that this estimate is very robust, because our results are based on a very *few* steps and assumptions. We assume that the metallicity of M 67 is essentially solar, and this is agreed on by all the latest works. We determined the $T_{\rm eff}$ in a differential way from the Sun, on spectra taken with the same instrument and using two sensitive methods (line-depth ratios and Hα wings). We prove that the stars are indeed very close to the Sun, showing how their spectra overlap with the solar one. The observed stars are still on the main sequence.

6. Cluster distance

The average V magnitude of the 10 solar analogs is 14.583 mag, which must be corrected for reddening: $A_V = 3.1 \times 0.041 = 0.127$, implying a de-reddened V magnitude

of 14.456. With a solar absolute V magnitude of 4.81 (Bessell et al. 1998), the distance modulus of M 67 is 9.65. As mentioned in the previous section, a correction might be needed if the metallicity differs substantially from the solar one (of up to 0.08 mag for [Fe/H] = 0.05, but we consider such a large difference in metallicity very unlikely). A correction of 0.002 mag, corresponding to a metallicity of [Fe/H] = 0.01 (used in the previous section) would bring to a distance modulus of 9.63.

This determination is in excellent agreement with two recent determinations: An et al. (2007) who estimate a distance modulus of 9.61, and Sandquist et al. (2004), who find 9.60, both using the same reddening as we adopted.

The associated error given by the spread around the average magnitude is 0.060 (i.e. $0.19/\sqrt{10}$) mag. Other sources of uncertainty in the distance modulus will be given by the error in reddening, which accounts for 0.012 mag, and by the uncertainty on [Fe/H]. If we assume an error on [Fe/H] of 0.03 dex, this accounts for 0.05 mag in the distance modulus. Summarizing, our best estimate of the distance modulus is $9.63 \pm 0.06_{\rm stat} \pm 0.05_{\rm sys}$.

A full comparison of our estimate with those present in literature is beyond the scope of this work. We do find remarkable the agreement between our distance estimate and the ones of Sandquist et al. (2004) and An et al. (2007), in particular when considering that our method is independent with of theirs.

7. Conclusion

By using selected observations with FLAMES/GIRAFFE at the VLT, we have made a convincing case that the open cluster M 67 hosts a number of interesting potential solar twins, and we have identified them. We computed spectroscopic accurate effective temperatures for all the stars with two methods. The color-temperature relationships we derived can be used to determine temperatures for MS solar-metallicity stars.

By computing the average solar twin colors, we have obtained a precise estimate of the solar $(B - V)$: $(B - V)_\odot = 0.649 \pm 0.016$. By averaging the magnitude of the solar twins, we have determined an accurate distance modulus for M 67: $9.63 \pm 0.06_{\rm stat} \pm 0.05_{\rm sys}$, which is in excellent agreement with the most recent estimates, based on different, independent methods and data sets.

We have determined Li abundances for all the stars, confirming the presence of a large Li spread among the solar stars of this cluster, but showing for the first time that the Li extra-depletion only appears in stars cooler than 6000 K. The candidate solar twins have Li abundance similar to that of our star, indicating that they also share the mixing history with the Sun.

Acknowledgements. We are grateful to F. Castelli for helping us understand how hydrogen profiles are computed in SYNTHE. K.B. was supported by the ESO DGDF 2006, and by the Italian *Ministero dell'Istruzione, Università e Ricerca* (MIUR) fundings. PB acknowledges support from EU contract MEXT-CT-2004-014265 (CIFIST). This research made use of SIMBAD and VIZIER databases, operated at the CDS (Strasbourg, France).

References

Ali, A. W., & Griem, H. R. 1965, Phys. Rev. 140, 1044
Ali, A. W., & Griem, H. R. 1966, Phys. Rev., 144, 366
Alonso, A., Arribas, S., & Martinez- Roger, C. 1996, A&A, 313, 873
An, D., Terndrup, D. M., Pinsonneault, M. H., et al. 2007, ApJ, 665, 233
Barklem, P. S., Stempels, H. C., Allende Prieto, C., et al. 2002, A&A, 385, 951
Barry, D. C., Cromwell, R., & Schoolman, S. A. 1978, ApJ, 222, 1032
Bessell, M. S., Castelli, F., & Plez, B. 1998, A&A, 333, 231
Biazzo, K., Frasca, A., Catalano, S., & Marilli, E. 2007, AN, 328, 938
Bonifacio, P., Molaro, P., Sivarani, T., et al. 2007, A&A, 462, 851
Carlsson, M., Rutten, R. J., Bruls, J. H. M., & Shchukina, N. G. 1994, A&A, 288, 860
Castelli, F., & Kurucz, R. L. 2001, A&A, 372, 260
Castelli, F., & Kurucz, R. L. 2003, in Modelling of Stellar Atmospheres, ed. N. Piskunov, W. W. Weiss, & D. F. Gray (ASP), Proc. IAU Symp., 210, 20
Catalano, S., Biazzo, K., Frasca, A., & Marilli, E. 2002, A&A, 394, 1009
Cayrel, R., Cayrel de Strobel, G., & Campbell, B. 1985, A&A, 146, 249
Cayrel, R. 1988, in The impact of very high S/N spectroscopy on Stellar Physics, ed. G. Cayrel de Strobel, & M. Spite (Kluwer), Proc. IAU Symp., 132, 345
Cayrel de Strobel, G. 1996, A&ARv, 7, 243
Cayrel de Strobel, G., & Bentolila, C. 1989, A&A, 211, 324
Charbonnel, C., & Talon, S. 2005, Science, 309, 2189
Cowley, C. R., & Castelli, F. 2002, A&A, 387, 595
Fuhrmann, K., Axer, M., & Gehren, T. 1993, A&A, 271, 451
Girardi, L., Bressan, A., Bertelli, G., & Chiosi, C. 2000, A&AS, 141, 371
Gratton, R., Bonifacio, P., Bragaglia, A., et al. 2001, A&A, 369, 87
Gray, D. F., & Johanson, H. L. 1991, PASP, 103, 439
Grevesse, N., & Sauval, A. J. 1998, Space Sci. Rev., 85, 161
Griem, H. R. 1960, ApJ, 132, 883
Holmberg, J., Flynn, C., & Portinari, L. 2006, MNRAS, 367, 449
King, J. R., Boesgaard, A. M., & Schuler, S. C. 2005, AJ, 130, 2318
Kurucz, R. 1993a, ATLAS9 Stellar Atmosphere Programs and 2 km s^{-1} grid. Kurucz CD-ROM No. 13. Cambridge, Mass.: Smithsonian Astrophysical Observatory
Kurucz, R. 1993b, SYNTHE Spectrum Synthesis Programs and Line Data. Kurucz CD-ROM No. 18. Cambridge, Mass.: Smithsonian Astrophysical Observatory
Mayor, M., & Queloz, D. 1995, Nature, 378, 375
Meléndez, J., & Ramírez, I. 2007, ApJ, 669, L89
Meléndez, J., Dodds-Eden, K., & Robles, J. A. 2006, ApJ, 641, L133
Montgomery, K. A., Kent, A., Marschall, L. A., & Janes, K. A. 1993, AJ, 106, 181
Müller, E. A., Peytremann, E., & de La Reza, R. 1975, Sol. Phys., 41, 53
Pace, G., Pasquini, L., Francois, P. 2008, A&A, 489, 403
Pasquini, L., Liu, Q., & Pallavicini, R. 1994, A&A, 297, 191
Pasquini, L., Randich, S., & Pallavicini, R. 1997, A&A, 325, 535
Pasquini, L., Avila, G., Blecha, A., et al. 2002, Msngr, 110, 1
Porto de Mello, G. F., & da Silva, L. 1997, ApJ, 482, L89
Randich, S. 2008, Mem. Soc. Astron. Italiana, 79, 516
Randich, S., Sestito, P., Primas, F., et al. 2006, A&A, 450, 557
Sanders, W. L. 1977, A&AS, 27, 89
Sandquist, E. L. 2004, MNRAS, 347, 101
Sbordone, L. 2005, MSAIS, 8, 61
Sbordone, L., Bonifacio, P., Castelli, F., & Kurucz, R. L. 2004, MSAIS, 5, 93
Soderblom, D. R., Jones, B. F., Balachandran, S., et al. 1993, AJ, 106, 1059
Soubiran, C., & Triaud, A. 2004, A&A, 418, 1089
Tautvaišiene, G., Edvardsson, B., Tuominen, I., & Ilyin, I. 2000, A&A, 360, 499
Taylor, B. J. 2007, AJ, 133, 370
Vidal, C. R., Cooper, J., & Smith, E. W. 1973, ApJS, 25, 37
Wilson, R. C., & Hudson, H. 1991, Nature, 351, 4
Yadav, R. K. S., Bedin, L. R., Piotto, G., et al. 2008, A&A, 484, 609

Appendix A: On line material

Table A.1. Object ID, coordinates (Equinox J2000, Epoch J2000.13), photometry, and proper motions of the targets (see Yadav et al. 2008, for details). In the last column the names of the stars according to Sanders (1977) or to Montgomery et al. (1993) are given. For a few stars, two names are given, because both stars are within 1 arc sec circle, according to SIMBAD database.

Object	α (°)	δ (°)	$B \pm \Delta B$ (mag)	$V \pm \Delta V$ (mag)	$I \pm \Delta I$ (mag)	$\mu_x \pm \Delta\mu_x$ (mas/yr)	$\mu_y \pm \Delta\mu_y$ (mas/yr)	Name
Obj219	132.893537	11.632623	13.715 ± 0.009	13.100 ± 0.008	12.425 ± 0.005	1.96 ± 1.31	8.63 ± 3.03	S1197
Obj266	132.860339	11.643584	14.212 ± 0.006	13.601 ± 0.006	12.939 ± 0.007	−0.24 ± 2.38	0.18 ± 3.45	S944
Obj285	132.849450	11.647816	15.165 ± 0.006	14.461 ± 0.000	13.713 ± 0.002	−0.42 ± 1.78	−2.80 ± 1.37	S945
Obj288	132.900657	11.648980	14.494 ± 0.013	13.857 ± 0.004	13.160 ± 0.005	0.00 ± 0.77	1.61 ± 2.44	S1201
Obj291	132.937203	11.649712	14.090 ± 0.010	13.478 ± 0.009	12.807 ± 0.018	0.18 ± 1.13	7.26 ± 3.03	S1202
Obj342	132.823311	11.660013	14.118 ± 0.004	13.503 ± 0.005	12.841 ± 0.008	0.77 ± 2.14	5.59 ± 4.22	S948
Obj349	132.979809	11.661163	14.978 ± 0.006	14.301 ± 0.002	13.614 ± 0.007	2.92 ± 8.87	2.92 ± 4.82	MMJ6241/S1423
Obj350	132.836621	11.661145	14.226 ± 0.005	13.624 ± 0.010	12.955 ± 0.006	−1.96 ± 1.07	0.18 ± 1.49	S950
Obj364	132.794912	11.664138	15.288 ± 0.005	14.584 ± 0.010	13.809 ± 0.006	−1.37 ± 1.55	0.24 ± 1.43	S951
Obj401	132.829348	11.671034	14.268 ± 0.006	13.661 ± 0.007	13.009 ± 0.003	−3.81 ± 2.56	1.31 ± 1.96	S954
Obj437	132.827827	11.676879	14.600 ± 0.006	13.998 ± 0.008	13.331 ± 0.002	2.98 ± 0.71	−2.02 ± 3.69	S956
Obj455	132.971225	11.681574	13.930 ± 0.007	13.301 ± 0.004	12.608 ± 0.018	5.30 ± 5.65	5.77 ± 2.80	S1428
Obj473	132.809740	11.685891	15.142 ± 0.011	14.443 ± 0.008	13.731 ± 0.004	1.31 ± 1.13	−1.55 ± 3.57	S958
Obj571	132.951947	11.706357	14.686 ± 0.012	14.021 ± 0.014	13.309 ± 0.004	−0.89 ± 1.31	−0.30 ± 3.21	S1211
Obj574	133.024207	11.706858	14.309 ± 0.016	13.653 ± 0.007	12.932 ± 0.005	−1.73 ± 1.01	−0.24 ± 1.07	MMJ6362/S1431
Obj587	132.911415	11.710387	14.753 ± 0.006	14.107 ± 0.006	13.405 ± 0.020	−0.89 ± 0.83	1.31 ± 3.15	S1213
Obj613	132.825417	11.715202	13.907 ± 0.015	13.254 ± 0.006	12.594 ± 0.022	1.78 ± 2.62	−0.89 ± 3.69	S964
Obj637	132.840991	11.721590	15.191 ± 0.017	14.489 ± 0.010	13.751 ± 0.011	0.65 ± 0.54	−0.42 ± 2.50	S966
Obj673	132.722266	11.727791	15.062 ± 0.002	14.356 ± 0.009	13.569 ± 0.001	0.00 ± 0.77	0.24 ± 2.86	S746
Obj681	132.773982	11.729705	14.715 ± 0.006	14.018 ± 0.016	13.254 ± 0.008	1.19 ± 1.31	1.49 ± 2.38	S747
Obj689	132.875550	11.730521	13.783 ± 0.012	13.120 ± 0.011	12.436 ± 0.010	−3.21 ± 2.86	−0.36 ± 3.87	S1219
Obj713	132.840699	11.734734	14.886 ± 0.017	14.172 ± 0.009	13.421 ± 0.017	1.55 ± 1.37	−0.48 ± 1.31	S969
Obj750	132.722677	11.742964	14.215 ± 0.007	13.576 ± 0.014	12.865 ± 0.005	0.18 ± 2.08	1.07 ± 2.20	S750
Obj756	132.947493	11.745099	15.393 ± 0.011	14.695 ± 0.008	13.923 ± 0.009	3.03 ± 0.89	5.06 ± 1.73	S1222
Obj769	132.959247	11.749185	14.119 ± 0.004	13.478 ± 0.003	12.771 ± 0.005	−0.36 ± 1.13	0.12 ± 2.98	S1224a
Obj778	132.836684	11.750684	13.716 ± 0.010	13.093 ± 0.011	12.411 ± 0.011	1.37 ± 1.78	2.98 ± 4.40	S976
Obj809	132.758539	11.755306	15.696 ± 0.007	14.959 ± 0.015	14.162 ± 0.004	−1.13 ± 1.61	−1.49 ± 1.84	S754
Obj851	132.854122	11.761931	14.730 ± 0.007	14.113 ± 0.004	13.449 ± 0.007	0.71 ± 3.09	2.98 ± 1.07	S982
Obj880	132.770112	11.765793	14.202 ± 0.009	13.544 ± 0.014	12.841 ± 0.002	−0.30 ± 1.07	−1.07 ± 1.61	S757
Obj905	132.746798	11.770272	14.038 ± 0.004	13.434 ± 0.010	12.748 ± 0.015	1.01 ± 1.73	−1.73 ± 2.74	S758
Obj911	132.791312	11.771367	15.220 ± 0.006	14.547 ± 0.010	13.785 ± 0.010	0.36 ± 1.31	1.19 ± 1.31	S991
Obj917	133.021288	11.772611	15.497 ± 0.007	14.755 ± 0.008	13.923 ± 0.006	−0.54 ± 2.56	2.44 ± 2.62	S1442
Obj971	132.884919	11.779352	15.287 ± 0.005	14.592 ± 0.004	13.793 ± 0.000	−0.12 ± 0.59	0.36 ± 0.30	S1246
Obj986	132.905212	11.782141	14.646 ± 0.008	14.007 ± 0.003	13.283 ± 0.001	0.24 ± 1.25	1.19 ± 0.54	S1247
Obj988	132.892171	11.782156	14.819 ± 0.005	14.180 ± 0.001	13.475 ± 0.002	−0.65 ± 0.65	−0.24 ± 1.49	S1248
Obj1010	132.850486	11.785927	14.104 ± 0.007	13.478 ± 0.009	12.781 ± 0.021	−0.36 ± 0.95	3.57 ± 1.43	S2209
Obj1032	132.985778	11.790265	14.997 ± 0.005	14.358 ± 0.003	13.649 ± 0.001	3.33 ± 3.33	−0.24 ± 0.48	S1449
Obj1036	132.851246	11.791211	15.678 ± 0.018	14.947 ± 0.003	14.164 ± 0.005	−0.36 ± 0.24	−1.01 ± 1.25	S1004
Obj1051	132.922899	11.793371	14.726 ± 0.007	14.090 ± 0.004	13.382 ± 0.004	−1.55 ± 0.54	1.96 ± 1.07	S1252
Obj1062	132.900316	11.796392	15.144 ± 0.001	14.477 ± 0.008	13.745 ± 0.004	1.25 ± 1.07	−0.12 ± 2.68	S1255
Obj1067	133.014592	11.796693	15.201 ± 0.005	14.559 ± 0.009	13.824 ± 0.002	0.24 ± 2.08	−0.30 ± 1.25	S1452
Obj1075	132.912716	11.798715	14.386 ± 0.000	13.712 ± 0.006	12.992 ± 0.004	1.19 ± 1.96	−2.80 ± 3.33	S1256
Obj1088	132.953942	11.800602	15.151 ± 0.004	14.492 ± 0.001	13.760 ± 0.007	0.77 ± 1.90	−3.99 ± 2.56	S1258
Obj1090	132.869575	11.800607	14.450 ± 0.004	13.800 ± 0.005	13.040 ± 0.010	0.18 ± 1.73	−1.55 ± 1.07	S1011
Obj1091	132.853518	11.801110	15.237 ± 0.011	14.513 ± 0.007	13.669 ± 0.008	0.12 ± 0.83	−0.48 ± 1.55	S1012
Obj1101	133.035214	11.802908	15.377 ± 0.001	14.675 ± 0.004	13.903 ± 0.001	−0.06 ± 1.31	−2.08 ± 2.50	MMJ6384
Obj1108	132.855293	11.803762	14.878 ± 0.005	14.177 ± 0.001	13.386 ± 0.006	−0.30 ± 0.95	−0.42 ± 0.71	S1014
Obj1129	132.885730	11.806694	14.795 ± 0.005	14.171 ± 0.006	13.482 ± 0.002	1.13 ± 0.30	−1.55 ± 1.31	S1260
Obj1137	132.800104	11.807413	15.571 ± 0.002	14.873 ± 0.008	14.107 ± 0.009	−1.90 ± 0.89	0.83 ± 1.19	S2213
Obj1161	132.981615	11.810602	14.549 ± 0.004	13.883 ± 0.010	13.149 ± 0.006	0.89 ± 4.46	−6.84 ± 2.86	S1457
Obj1163	132.787098	11.810483	14.688 ± 0.009	13.992 ± 0.004	13.221 ± 0.002	0.42 ± 0.65	8.03 ± 1.19	S1022
Obj1194	132.753356	11.814655	15.281 ± 0.002	14.614 ± 0.010	13.876 ± 0.002	0.30 ± 1.01	−0.42 ± 0.65	S770
Obj1197	132.877372	11.815215	13.921 ± 0.006	13.315 ± 0.003	12.618 ± 0.024	−0.18 ± 1.07	1.78 ± 0.77	MMJ5882/S1264b
Obj1247	132.812708	11.822522	14.753 ± 0.008	14.144 ± 0.008	13.470 ± 0.005	0.65 ± 1.25	−2.80 ± 1.96	S1033
Obj1303	132.736097	11.831844	15.318 ± 0.008	14.641 ± 0.008	13.899 ± 0.009	0.06 ± 2.26	0.89 ± 1.25	S779
Obj1304	132.858515	11.832075	15.454 ± 0.015	14.731 ± 0.009	13.916 ± 0.006	−0.12 ± 1.31	−0.12 ± 1.90	S1041
Obj1315	132.994897	11.834025	14.990 ± 0.013	14.297 ± 0.011	13.544 ± 0.008	−1.19 ± 4.40	0.48 ± 2.20	MMJ6306/S1462
Obj1334	132.866453	11.836636	15.083 ± 0.007	14.403 ± 0.007	13.669 ± 0.000	0.77 ± 1.61	−1.84 ± 0.89	S1048
Obj1342	132.826093	11.838787	14.935 ± 0.006	14.285 ± 0.005	13.547 ± 0.001	1.37 ± 1.49	−0.36 ± 0.06	S1050
Obj1387	132.874854	11.852505	14.724 ± 0.004	14.098 ± 0.002	13.398 ± 0.000	0.59 ± 3.75	−1.55 ± 7.97	S1283
Obj1392	132.749200	11.853500	15.527 ± 0.002	14.811 ± 0.004	14.047 ± 0.000	−1.49 ± 2.08	−1.61 ± 0.77	S785
Obj1397	132.882992	11.854616	14.631 ± 0.001	14.009 ± 0.003	13.304 ± 0.001	1.84 ± 2.32	−3.03 ± 5.89	S1287
Obj1424	132.890226	11.862493	13.825 ± 0.009	13.203 ± 0.005	12.501 ± 0.000	1.49 ± 2.50	−1.25 ± 3.87	Check
Obj1458	132.762475	11.873808	15.716 ± 0.010	14.977 ± 0.005	14.186 ± 0.004	1.01 ± 1.84	0.12 ± 1.49	S795
Obj1480	132.916988	11.878716	14.383 ± 0.008	13.783 ± 0.008	13.125 ± 0.002	−3.99 ± 2.50	1.25 ± 2.32	S1300
Obj1496	132.781325	11.882262	14.486 ± 0.013	13.879 ± 0.004	13.214 ± 0.002	−0.95 ± 0.12	−0.30 ± 0.65	S2224
Obj1504	132.864557	11.884028	14.796 ± 0.001	14.171 ± 0.011	13.474 ± 0.000	−1.13 ± 0.95	1.31 ± 1.31	S1078

Table A.1. continued.

Object	α (°)	δ (°)	$B \pm \Delta B$ (mag)	$V \pm \Delta V$ (mag)	$I \pm \Delta I$ (mag)	$\mu_x \pm \Delta\mu_x$ (mas/yr)	$\mu_y \pm \Delta\mu_y$ (mas/yr)	Name
Obj1514	132.753181	11.886527	15.498 ± 0.003	14.777 ± 0.004	14.008 ± 0.000	−0.12 ± 1.13	1.73 ± 1.37	S802
Obj1587	132.846438	11.901394	14.804 ± 0.015	14.163 ± 0.004	13.469 ± 0.006	−0.95 ± 1.73	−1.01 ± 1.78	S1087
Obj1622	132.801216	11.906389	14.788 ± 0.004	14.156 ± 0.002	13.459 ± 0.004	1.43 ± 1.25	0.95 ± 0.65	S1089
Obj1680	132.883591	11.919069	14.291 ± 0.015	13.646 ± 0.006	12.951 ± 0.004	1.01 ± 1.13	0.18 ± 1.07	S1314
Obj1706	133.010317	11.926166	15.468 ± 0.005	14.745 ± 0.017	13.981 ± 0.006	0.54 ± 0.95	0.30 ± 0.54	MMJ6341/S1481
Obj1716	132.866205	11.928044	13.918 ± 0.010	13.299 ± 0.009	12.625 ± 0.005	−1.96 ± 1.84	4.82 ± 3.15	S1092
Obj1722	132.828014	11.930478	14.731 ± 0.002	14.130 ± 0.006	13.449 ± 0.009	−3.57 ± 26.24	−2.44 ± 2.20	S1093
Obj1735	133.001728	11.935288	14.993 ± 0.012	14.332 ± 0.010	13.617 ± 0.007	1.96 ± 1.78	−2.92 ± 1.55	S1483
Obj1758	132.746824	11.943570	13.860 ± 0.056	13.207 ± 0.015	12.545 ± 0.007	−0.89 ± 0.48	3.45 ± 1.67	MMJ5342/S816
Obj1768	132.906577	11.945718	15.060 ± 0.003	14.404 ± 0.004	13.684 ± 0.004	0.77 ± 1.13	−1.01 ± 0.89	MMJ6028/S1320
Obj1778	132.737778	11.947424	15.679 ± 0.004	14.948 ± 0.004	14.155 ± 0.003	0.83 ± 1.96	−0.65 ± 0.65	MMJ5310/S820
Obj1787	132.788102	11.950097	15.214 ± 0.006	14.547 ± 0.004	13.813 ± 0.003	1.61 ± 1.73	2.26 ± 2.26	MMJ5484
Obj1788	132.804106	11.950254	15.104 ± 0.008	14.441 ± 0.004	13.709 ± 0.000	−1.78 ± 1.13	4.64 ± 1.84	MMJ5541
Obj1842	132.786897	11.964913	14.844 ± 0.007	14.237 ± 0.002	13.557 ± 0.005	−0.36 ± 1.01	−1.61 ± 1.49	MMJ5479/S1102
Obj1852	133.013763	11.967948	14.575 ± 0.011	13.962 ± 0.008	13.286 ± 0.005	−1.01 ± 2.32	1.67 ± 3.51	S1486
Obj1862	132.743111	11.970785	15.126 ± 0.001	14.483 ± 0.003	13.753 ± 0.004	−0.06 ± 1.37	0.89 ± 1.13	MMJ5331
Obj1903	132.783150	11.981489	15.422 ± 0.004	14.733 ± 0.003	13.971 ± 0.001	−1.67 ± 1.25	0.83 ± 0.83	MMJ5469
Obj1948	132.928314	11.991953	14.627 ± 0.009	14.015 ± 0.004	13.327 ± 0.002	0.42 ±1.67	−3.45 ± 2.98	S1330
Obj1955	132.743729	11.994304	14.842 ± 0.001	14.212 ± 0.004	13.483 ± 0.002	0.59 ±0.54	−2.98 ± 3.39	MMJ5338/S829
Obj1957	132.888539	11.994779	14.406 ± 0.007	13.789 ± 0.004	13.085 ± 0.008	−1.19 ± 1.90	0.18 ± 3.69	MMJ5962/S1331
Obj2016	132.931975	12.015297	14.158 ± 0.002	13.553 ± 0.007	12.841 ± 0.000	0.77 ±2.38	0.30 ± 2.44	S1333
Obj2017	132.943039	12.015413	15.509 ± 0.003	14.857 ± 0.001	14.109 ± 0.001	−2.68 ± 2.62	6.90 ± 3.87	S1334
Obj2018	132.914220	12.015883	15.237 ± 0.000	14.565 ± 0.005	13.832 ± 0.007	−2.50 ± 1.55	1.67 ± 2.02	MMJ6055

Table A.2. Radial velocities, effective temperatures, and lithium abundances of the 59 stars retained as possible single members. The values in Table are derived by adding the difference of $T_{\rm eff}$ between the stars and the Sun to the solar temperature (5777 K). The solar temperature derived from the GIRAFFE spectrum and our calibrations is 5792 and 5717 K for the LDR and Hα methods, respectively. The 10 best solar twin candidates are indicated in bold face. The S/N /pixel of the co-added spectra varies between 80 and 110, depending on the magnitude of the stars.

Object	$V_{\rm rad} \pm \Delta V_{\rm rad}$ (km s^{-1})	$T_{\rm eff}^{\rm LDR} \pm \Delta T_{\rm eff}^{\rm LDR}$ (K)	$T_{\rm eff}^{\rm H\alpha}$ (K)	$EW_{\rm Li+Fe}$ (mÅ)	log $EW_{\rm Li}$ (mÅ)	log N(Li)$^{\rm LTE}$	log N(Li)$^{\rm NLTE}$
Sun		5777 ± 27	5777	12.1	0.3	0.8	0.8
219	33.85 ± 0.28	6243 ± 54	6110	22.7	1.2	2.1	2.1
266	32.95 ± 0.46	6147 ± 63	6060	53.2	1.7	2.6	2.5
285	33.72 ± 0.67	5836 ± 67	5777	1.5	<0.0	0.6	<0.6
288	34.26 ± 0.40	6004 ± 67	6010	42.4	1.5	2.3	2.3
291	32.13 ± 0.29	6177 ± 57	6160	59.6	1.7	2.6	2.6
349	34.28 ± 0.42	5952 ± 78	5917	10.4	<0.0	0.7	<0.7
350	32.56 ± 0.31	6024 ± 52	6010	68.2	1.8	2.6	2.6
401	32.64 ± 0.37	6165 ± 64	6110	44.9	1.6	2.5	2.4
473	34.74 ± 0.38	5919 ± 76	5807	2.7	<0.0	0.7	<0.7
587	33.06 ± 0.39	6077 ± 65	6060	37.2	1.4	2.3	2.3
613	33.05 ± 0.29	6202 ± 45	6110	61.3	1.7	2.7	2.6
637	34.00 ± 0.50	5806 ± 65	5777	17.8	0.9	1.4	1.4
673	32.44 ± 0.57	5639 ± 63	5747	19.1	0.9	1.4	1.4
689	32.88 ± 0.24	6093 ± 41	6110	42.3	1.5	2.4	2.3
750	33.13 ± 0.28	5918 ± 48	5927	16.4	0.9	1.5	1.5
769	34.47 ± 0.29	5984 ± 46	6010	29.4	1.3	2.1	2.0
778	33.45 ± 0.24	6114 ± 39	6060	15.6	0.8	1.7	1.7
809	31.87 ± 0.48	5667 ± 78	5537	6.9	<0.0	0.4	<0.5
851	33.47 ± 0.31	5948 ± 61	6060	12.9	0.6	1.3	1.3
911	32.08 ± 0.35	5885 ± 67	5837	13.4	0.6	1.2	1.2
988	32.07 ± 0.28	5935 ± 53	6060	28.2	1.3	2.0	2.0
1032	34.02 ± 0.47	5955 ± 60	6010	17.8	0.9	1.6	1.6
1036	33.39 ± 0.48	5612 ± 66	5537	20.9	1.0	1.4	1.4
1051	32.21 ± 0.29	6081 ± 55	6060	34.7	1.4	2.2	2.2
1062	32.64 ± 0.45	5926 ± 55	5867	21.0	1.1	1.7	1.7
1067	33.37 ± 0.35	5929 ± 69	5917	11.4	0.4	1.0	1.0
1075	33.13 ± 0.24	5871 ± 48	5917	10.7	0.0	0.6	0.7
1088	32.87 ± 0.29	5890 ± 59	5867	9.3	<0.0	0.6	<0.7
1090	33.34 ± 0.32	6086 ± 54	6010	41.2	1.5	2.3	2.3
1101	32.72 ± 0.34	5756 ± 60	5717	6.9	<0.0	0.5	<0.6
1129	33.92 ± 0.30	5959 ± 51	6010	32.4	1.4	2.1	2.1
1137	33.59 ± 0.48	5741 ± 69	5627	5.3	<0.0	0.5	<0.6
1194	33.30 ± 0.40	5766 ± 64	5837	5.3	<0.0	0.5	<0.6
1197	34.26 ± 0.28	6207 ± 44	6110	28.1	1.3	2.2	2.2
1247	32.44 ± 0.51	5994 ± 60	6010	30.2	1.3	2.1	2.1
1303	32.65 ± 0.41	5716 ± 64	5717	10.1	<0.0	0.5	<0.6
1304	33.60 ± 0.39	5704 ± 64	5717	7.9	<0.0	0.5	<0.5
1315	32.55 ± 0.34	5874 ± 58	5867	15.6	0.8	1.4	1.4
1334	32.37 ± 0.45	5957 ± 57	5957	29.2	1.3	2.0	2.0
1387	33.35 ± 0.24	6090 ± 58	6060	37.5	1.5	2.3	2.3
1392	33.68 ± 0.57	5716 ± 63	5687	6.3	<0.0	0.5	<0.6
1458	32.55 ± 0.56	5640 ± 65	5567	6.1	<0.0	0.4	<0.5
1496	34.22 ± 0.48	6173 ± 54	6160	63.1	1.7	2.7	2.6
1504	33.39 ± 0.48	5934 ± 56	6060	40.7	1.5	2.2	2.2
1514	33.33 ± 0.49	5613 ± 67	5597	25.6	1.2	1.6	1.6
1587	32.38 ± 0.62	5975 ± 55	6010	28.6	1.3	2.0	2.0
1622	33.26 ± 0.61	6043 ± 57	6010	34.6	1.4	2.2	2.2
1716	33.84 ± 0.59	6030 ± 40	6060	40.8	1.5	2.3	2.3
1722	33.87 ± 0.52	6007 ± 62	6010	38.1	1.5	2.3	2.2
1735	33.18 ± 0.59	5959 ± 59	5960	10.9	0.2	0.9	0.9
1758	33.78 ± 0.67	6221 ± 52	6160	36.3	1.4	2.4	2.4
1768	33.98 ± 0.57	5844 ± 57	5927	40.1	1.5	2.1	2.1
1787	33.44 ± 0.57	5768 ± 70	5807	12.9	0.5	1.1	1.0
1788	33.38 ± 0.80	5886 ± 60	5867	23.4	1.1	1.8	1.8
1852	32.30 ± 0.40	6009 ± 63	6010	32.2	1.4	2.1	2.1
1903	32.76 ± 0.42	5609 ± 72	5687	6.8	<0.0	0.4	<0.5
1948	32.86 ± 0.29	6164 ± 63	6010	43.0	1.5	2.4	2.4
1955	32.63 ± 0.60	5961 ± 76	5837	35.8	1.4	2.2	2.2
2018	31.78 ± 0.43	5693 ± 74	5777	8.7	<0.0	0.4	<0.5

Table A.3. Radial velocities of likely binaries or non members. For these stars, each of the three RV measurements is given. Fields with blanks indicate that problems were present with the cross-correlation profile of these objects.

Object	$V^1_{\rm rad}$	$\Delta V^1_{\rm rad}$	$V^2_{\rm rad}$	$\Delta V^2_{\rm rad}$	$V^3_{\rm rad}$	$\Delta V^3_{\rm rad}$
342	17.74	0.72	57.20	1.45	40.75	0.73
364	36.93	0.43	36.58	1.18	36.48	0.74
437	45.87	0.65	45.54	0.83	45.68	0.52
455	38.07	0.50	14.62	1.24	33.41	0.47
571	31.73	0.49	31.07	0.66	31.47	0.56
574	42.88	0.46	42.91	0.85	42.08	0.62
681	24.14	0.80	56.70	1.22	59.70	0.85
713	35.34	0.46	35.03	0.64	34.91	0.33
756	46.24	0.50	45.54	0.77	45.47	0.41
880	39.62	6.67	/	/	33.55	5.81
905	34.78	0.35	37.30	1.02	74.65	0.89
917	18.66	0.86	15.59	1.36	/	/
971	36.13	0.51	36.13	0.70	36.22	0.63
986	16.54	0.53	27.69	0.84	49.08	0.68
1010	17.22	0.97	30.77	0.63	34.29	0.75
1091	27.59	3.27	27.03	0.62	25.77	0.78
1108	15.92	1.00	/	/	/	/
1161	35.53	0.65	35.49	1.21	22.45	1.55
1163	10.10	0.66	65.99	1.32	70.80	1.24
1342	37.97	0.69	28.40	1.06	34.93	0.65
1397	35.43	1.12	34.91	0.85	34.88	0.54
1424	54.44	1.62	57.22	1.31	56.04	1.58
1480	22.86	1.02	25.56	1.09	28.27	0.48
1680	37.65	1.29	35.65	0.96	32.27	0.81
1706	35.79	1.05	35.40	0.90	35.77	0.61
1778	29.59	1.30	29.92	2.96	31.19	1.26
1842	30.09	0.69	29.88	1.20	30.52	0.47
1862	31.31	0.63	30.29	2.03	31.27	0.43
1957	21.17	0.52	20.15	0.83	21.21	0.57
2016	21.64	0.46	25.96	0.94	65.63	0.66
2017	126.58	0.84	125.09	1.62	126.01	0.63